Hoeche, D.; Blawert, C.; Cavellier, M.; Busardo, D.; Gloriant, T.**:**
Magnesium nitride phase formation by means of ion beam implantation technique
In: Applied Surface Science (2011) Elsevier

DOI: 10.1016/j.apsusc.2011.01.061

Magnesium nitride phase formation by means of ion beam implantation technique

Daniel Höche[a], Carsten Blawert[a], Matthieu Cavellier[b,c], Denis Busardo[b], Thierry Gloriant[c]

[a] *Helmholtz-Zentrum Geesthacht Zentrum für Material- und Küstenforschung GmbH , Institute of Materials Research, Max-Planck-Strasse 1, D-21502 Geesthacht, Germany*
[b] *Quertech Ingenierie, Rue de la Girafe 9, F-14000 CAEN, France*
[c] *INSA Rennes, UMR CNRS 6226 Sciences Chimiques de Rennes / Chimie-Mtallurgie, Avenue des buttes de Coesmes 20, F-35043 Rennes, France*

Abstract

Nitrogen implantation technique (Hardion$^+$) has been applied in order to modify the surface properties of magnesium and Mg- based alloys (AM50, AZ31). Nitrogen ions with an energy of approximately 100 keV were used to form the Mg_3N_2 phase leading to improved surface properties. The samples were investigated using various characterization methods. Mechanical properties have been tested by means of nanoindention, the electrochemical behavior was measured by potentiodynamic polarization and impedance spectroscopy, phase formation by using grazing incidence Xray diffraction, the chemical state was determined by means of Xray induced photoelectron spectroscopy (XPS) and depth profiling by using secondary ions mass spectroscopy (SIMS). Additionally, the results were compared to calculated depth profiles using SRIM2008. The correlation of the results shows the nitride formation behavior to a depth of about 600 nm.

Keywords: Magnesium nitride, Ion implantation, XPS, Corrosion

1. Introduction

Ion implantation is a well-known process to improve metals surface properties. One of the easiest and the most efficient ion to implant is nitrogen.

Email address: Daniel.Hoeche@hzg.de ()
[1]phone:++49 4152-87 1914

Due to the formation of metals nitrides, nitrogen implantation leads to significant results, enhancing corrosion resistance [1, 2, 3, 4] or mechanical properties [4, 5, 6, 7, 8, 9, 10, 11]. However, most of nitrogen ion implantation experimentations were made on steels, aluminium, titanium and zirconium alloys. The arising new surface properties induced by nitrogen implantation make these implanted metals very useful in many industrial applications [10, 11, 12].
Magnesium alloys are interesting for the industries where weight gain is the priority; unfortunately, their poor corrosion resistance has delayed its use in many applications [13, 14, 15]. Concerning the known possibilities and based on prior works of researchers [16, 17, 18] the nitriding of magnesium, its corrosion resistance enhancement, the phase formation and the changes of mechanical properties due to nitrogen ion implantation have been studied and evaluated.

2. Experimental

2.1. Sample preparation

Pure magnesium (99.92% purity) pieces (2cm x 2cm) were separated from cast magnesium blocks and have been grinded and polished using emery paper (2400) including careful cleaning. The AM50 (5.66.4 wt.% Al, 0.260.5 wt.% Mn, 0.1-0.2 wt.% Zn, Mg bal.) and AZ31 (2.5-3.5 wt.% Al, 0.6-1.4 wt.% Zn, 0.1-0.2 wt.% Mn, Mg bal.) pieces were taken from commercial sheets and have been prepared like the pure magnesium before. Directly before ion implantation, samples were polished mechanically with SiC paper (up to grit P-4000), cleaned in ethylic alcohol in an ultrasound bath and dried immediately.

2.2. Hardion$^+$ implantation process

Nitrogen implantation was performed using the micro-implanter developed and patented by Quertech Ingnierie. This equipment is mainly composed of an ECR (Electron Cyclotron Resonance) ion source coupled to a vacuum chamber. According to Lius work [3], samples were implanted with 65keV N^+ ions at a fluence of $4 \cdot 10^{17} ions/cm^2$ by means of an accelerator. The resulting average beam energy due to multiple charges (and at least different accelerations) is approx. 100 keV. After implantation the depth profile is a superposition of five separate "single or normal" distributions.

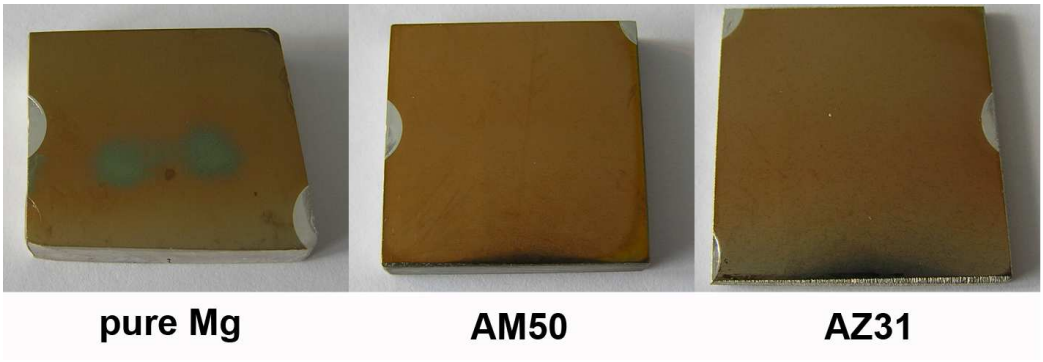

Figure 1: Irradiated samples after Hardion$^+$ technology treatments.

2.3. Analysis

SIMS. Secondary ion mass spectroscopy (SIMS) experiments were done on a Hiden Analytical system including the IG20 ion gun using Ar^+ ions at 5 keV and a MAXIM - Quadrupole mass detector. The focused beam has a diameter of 100 microns containing 500 nA current. To avoid edge effects at the crater the beam was rasterised (area 2 mm^2) across the Mg sheets. Signals were just measured in the inner gate of 0.5 mm^2. The sputter rate was approx. 12 nm per minute for total sputter times of 5400 s ($\approx$ 1 micron). In order to get the magnesium nitride distribution mass 38 (MgN^-) was applied.

XPS. X-ray induced photoelectron spectroscopy (XPS) experiments were carried out on a Kratos Axis Ultra DLD attached with a 15 kV X-ray gun using monochromatic Al K_α radiation. The spot size was 700 x 300 microns and the pass energy 40 eV at the regions measurements. Due to physical limits the information depth is limited to approx. 5 nm. Additionally, argon ions (4 keV) have been used to etch the samples for different times in order to obtain depth profiles. The used sputter rate was approx. 36 nm per minute for total sputter times of 1320 s ($\approx$ 800 nm). By determination of the binding energy on Mg 2p, N 1s, Al 2p, C 1s and O 1s states, the present chemical bonds have been accurately determined.

XRD. X-ray diffraction (XRD) has been performed on a Panalytical system including a thin film attachment and an "Euler" circle using CuK_α radiation. The scans have been carried out at grazing incidence geometry (3) leading to an information depth of approximately seven microns.

Corrosion. Corrosion tests were performed on both untreated and N implanted CP-Mg, AZ31 and AM50 magnesium alloys in ground (up to 2400 grid) and as implanted condition. All specimens were cleaned in alcohol prior to corrosion test. Electrochemical experiments were performed in 0.5% NaCl solution at pH 6.5, saturated with atmospheric oxygen. The corrosion cell (333 ml) with a three electrode set-up consisted of an Ag/AgCl reference, a Pt counter electrode and the specimen as working electrode. The electrolyte temperature was 22 $\pm$ 0.4°C and the electrolyte was stirred during the experiments. On one half of the specimens potentiodynamic polarisation and on the second half electrochemical impedance spectroscopy (EIS) measurements were performed. Please note that the number of specimens for corrosion testing was limited, thus only one polarisation and one impedance measurement was performed for each material/surface condition. Therefore the corrosion results can be only considered as a preliminary study and would require more measurements to ensure the trend statistically. The polarisation measurement started with 30 minutes recording of the free corrosion potential followed by the potential scan from -200 mV relative to the free corrosion potential with a scan rate of 0.2 mV/s. The test was terminated when a corrosion current of 0.1 mA was exceeded to minimize the damage on the specimen surface. From the cathodic branch of the polarization curve the corrosion rate was determined using the current density at the intersection of the Tafel slope with the vertical through the corrosion potential. The impedance spectroscopy at free corrosion potential was carried out using a Gill AC over the frequency range from 10 kHz to 0.01 Hz. The amplitude of the sinusoidal signals was 10 mV. The first measurement started 300 s after immersion into the 0.5% NaCl solution and was repeated at certain fixed times to follow the degradation of the surface. The charge transfer resistance was taken at the intersection of the Nyquist Plot with the real axis (corrected by the solution resistance) representing the direct current ohmic resistance.

Hardness. Hardness was measured by nanoindentation. The nano-indentor was equipped with a Berkovich diamond tip. In order to plot a continuous depth-hardness profile, measurements were made using an oscillating mode, with 2 mN increasing steps. This mode permits to measure hardness for each 2 mN step. For each sample, ten measurements were made to plot the average hardness profile, before and after ion implantation.

3. Results

3.1. Coating formation

The treatments lead to golden color like surfaces shown in figure 1. In order to determine the chemical state and the elemental distribution several different analysis methods were applied. Additionally, SRIM2008 [19] calculations have been carried out in a rough approximation for a better understanding of the formation process. Therefore nitrogen ions of an energy of 100 keV were assumed during the calculation. Pure magnesium (density 1.74 g/cm^3) was used as matrix material. Figure 2 shows the simulation results after 10^5 events. As expected, the maximum N content is far from the surface at about 300 nm in depth.

On top a passivation layer of MgO was formed. This some nanometer thick region avoids the decomposition of the nitride in air [20] due to the humidity and the arising reactions forming NH_3 and MgO described by the following equation:

$$Mg_3N_2 \; + \; 3H_2O \; \rightarrow \; 3MgO \; + \; 2NH_3 \tag{1}$$

The passivation film was observed for all samples very well by means of SIMS and XPS in figure 3 and 4. The transition from oxide to nitride regions has an interdiffusion like character arising from the coating formation and from the ion trajectories.

SIMS depth profiling reveals a lot of information about the coatings itself. It is important to mention that just depth profiles can be measured not absolute concentrations. The high count rate at the beginning is a result of surface effects influencing the method. After some seconds the sputter process reached equilibrium and became meaningful. The negative ion profiles show the surface carbon contaminations on all samples of some nanometers. Below, the oxides become visible up to a sputter time of 800 s corresponding to a depth of about 150 nm. It is slightly thicker for the aluminium containing alloys which lead to the assumption of Al_2O_3 formation, which will be verified in figure 5.

Carbon and oxygen are rapidly slowing down in depth, but it is really interesting to observe the nitrogen distribution. The N atoms are mostly in bond with the magnesium leading to a weak and total different N- signal compared to MgN^-. Thus, the nitride profile can be measured by means of MgN^- ions. The Mg_3N_2 develops in a depth between 150 nm and 600 nm. This is in good agreement with the SRIM2008 calculations. The width of the distribution is

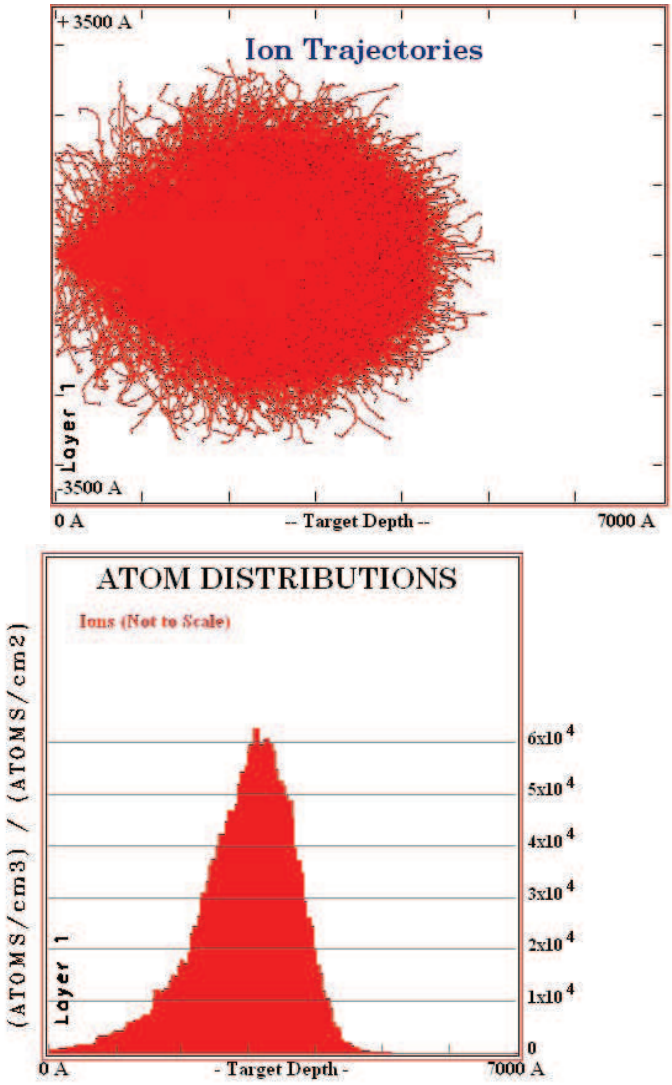

Figure 2: SRIM2008 depth profile calculation using 100 keV N ions. The first figure shows the trajectories and the second one the final elemental distribution for one state.

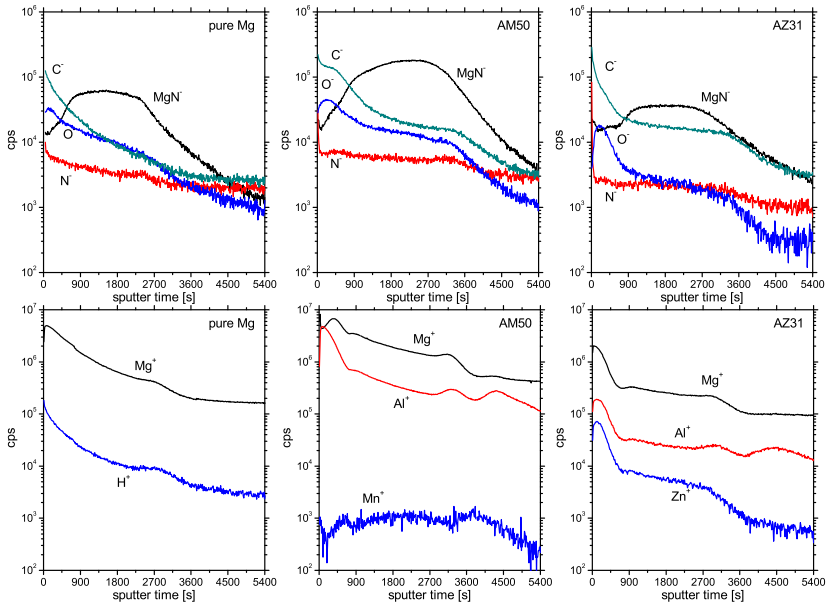

Figure 3: Negative and positive ions SIMS depth profiles of N implanted pure Mg, AM50 and AZ31 measured at same conditions for 5400 s.

larger in reality. Due to the phase formation the implanting conditions were changed during the treatments, which is not considered in the simulation. The positive ion depth profiles show the enrichment of alloying elements at the alpha- Mg and nitride interface and at the passivation film, which was expected. The decrease of all signals results from changes in the sputter rate due to the variation in the chemical composition.

In order to get the chemical states high resoluted XPS spectra have been measured at the Mg 2p, N 1s, O 1s, Al 2p and C 1s binding energy. The phase depth profiles verify the SIMS measurements. The binding energy of N 1s was measured to be 396.4 eV and 50.3 eV for Mg 2p in Mg_3N_2 after energy calibration using Au 4f signals. That shows that all nitrogen atoms are in chemical bond to magnesium or aluminium, excepting the surface contaminations with carbon (figure 6). In the case of AM50 and AZ31, AlN was observed too at a binding energy of N 1s of 397.2 eV (literature 397.0 eV [21]). It will be shown later that this significant influences the chemical and mechanical properties. Similar investigations have been carried out in [22] on magnesium nitride films deposited by pulsed laser deposition. They determined the exact same binding energies.

The formation of a MgO passivation film on the samples was observed

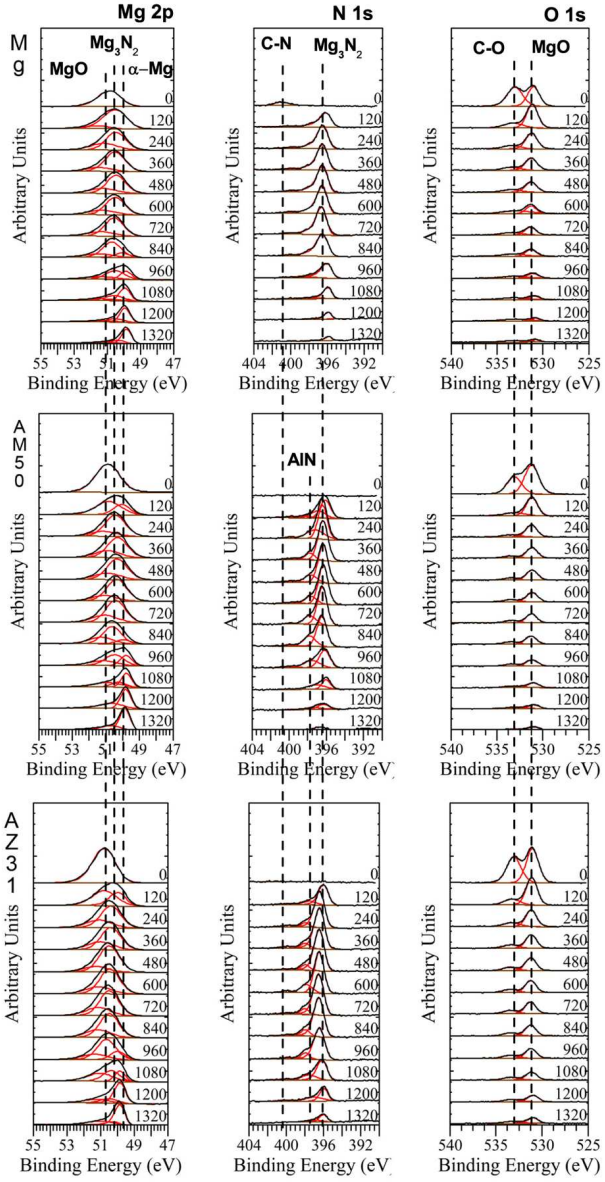

Figure 4: XPS depth profiles of N implanted pure Mg, AM50 and AZ31 for the Mg 2p, N 1s and O 1s state sputtered for 1320 s ($\approx$ 800 nm).

on the O 1s level at 531 eV (literature 531 - 530 eV [23]). Its importance for the method has been described earlier. The diffusion like decrease in O content becomes visible in the depth profiles too. Additionally, the formation of Al_2O_3 arises for Al containing alloys. The Al 2p state in figure 5 shows the peak shift due to oxide and nitride formation at 75.2 eV and 73.9 eV binding energy (literature 75.7 eV and 74.2 eV (Al 72.8 eV) [24]). The C 1s state shown in figure 6 was measured to study contamination effects. Due to the air exposure C-O / C-H compounds are at the surface. After sputtering a small amount of C-N bonded atoms become visible. The carbon is an artefact of contamination during implantation as a result of C-N collisions.

The Mg 2p and Al 2p peaks have been deconvoluted by means of Gauss-Lorentz GL(30) peak functions and Shirley backgrounds [25], in order to get depth profiles of compounds. Figure 7 presents the results. The influence of carbon (C 1s) peak was neglected. Compared to SIMS a good correlation was found. The AlN distributions is similar to the Mg_3N_2 depth profile. The high amount of AlN is a result of the stoichiometric factors: 1 Al to 3 Mg.

3.2. Phase detection

The crystallographic structure was measured at grazing incidence X-ray diffraction at 3° leading to an information depth of about seven microns (calculated from [26]). This is still very much and leads to a strong superposition of the bulk signal on the coating pattern because of its thickness

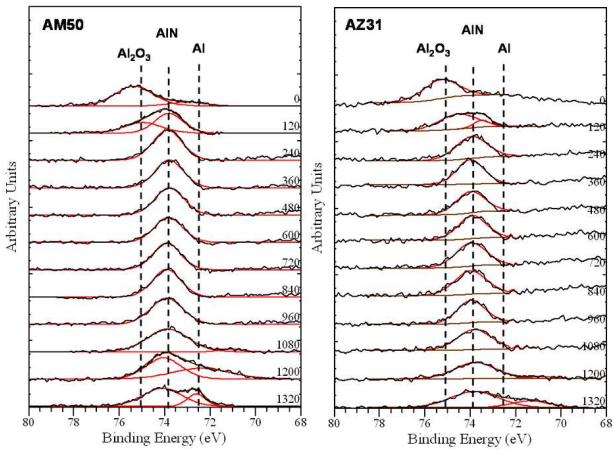

Figure 5: XPS depth profiles of N implanted pure AM50 and AZ31 for the Al 2p state sputtered for 1320 s (≈ 800 nm).

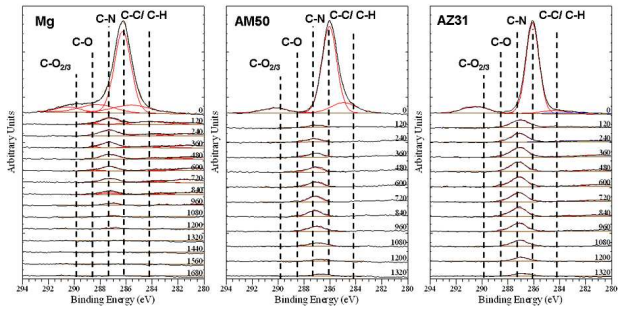

Figure 6: XPS depth profiles of N implanted pure Mg, AM50 and AZ31 for the C 1s state sputtered for 1320 s ($\approx$ 800 nm).

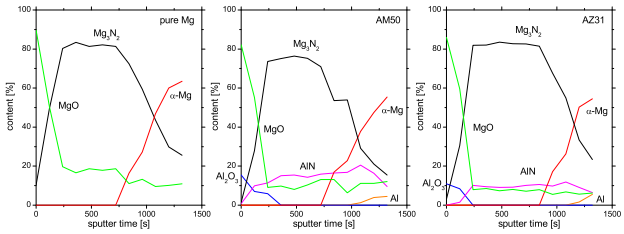

Figure 7: Depth profiles of chemical compounds of N implanted pure Mg, AM50 and AZ31 after the deconvolution of Al,Mg 2p states.

of only about 500 nm. Figure 8 plots the diffraction pattern of all samples. As mentioned above the signals arising from the hexagonal bulk material are dominant. The peak intensities are also correlated to the texture which is clear due to the manufacturing processes of the raw material. They correspond to the ICDD Pdf number 01-071-3765. In addition the cubic Mg_3N_2 (ICDD Pdf number 00-035-0778) has been indicated. It is possible to identify the phase by comparing the pattern with the untreated one. Especially in the 2Θ range around 20°and 38°-45° the differences become visible. The peaks are weak and evaluation becomes very difficult. Taking the shape and width into account it can be supposed that according to Debye-Scherrer formula [27] the crystallite size is smaller than 20 nm (nano-crystalline). Even at some 2 theta values the background is very strong. It is possible that amorphous structures have been developed during the treatments. AlN and other possible compounds do not have been measured due to the low amount in the interacting regions and the undergoing of the detection limit.
Obviously, the comparison of pure Mg, AM50 and AZ31 diffraction pattern

Table 1: Corrosion rates (mm/year) in neutral 0.5% NaCl solution determined by potentiodynamic polarisation measurements.

Alloy /corrosion rate (mm/year)	as received	N implanted
CP-Mg	1.56	0.99
AM50	0.4	0.92
AZ31	0.4	0.65

reveals the increase of crystallization rate with increasing aluminum content. It can be supposed that Al and other alloying elements support heterogenous nucleation.

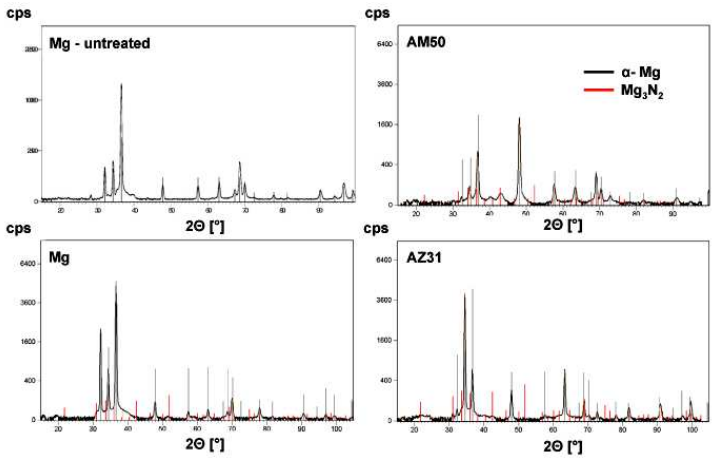

Figure 8: 3° grazing incidence diffraction pattern of untreated Mg and all N- ion implanted magnesium and alloy systems.

3.3. Corrosion properties

The results of the polarisation measurements are presented in Fig. 9 and Tab. 1. From the results it is obvious that only the treated CP-Mg reveals an improvement in the corrosion resistance after nitrogen implantation compared to the untreated substrate. None of specimen regardless of the surface condition shows a remarkable retardation of the anodic dissolution after passing the corrosion potential. Thus nitrogen appears to have no effect on the passive behavior of magnesium alloys.

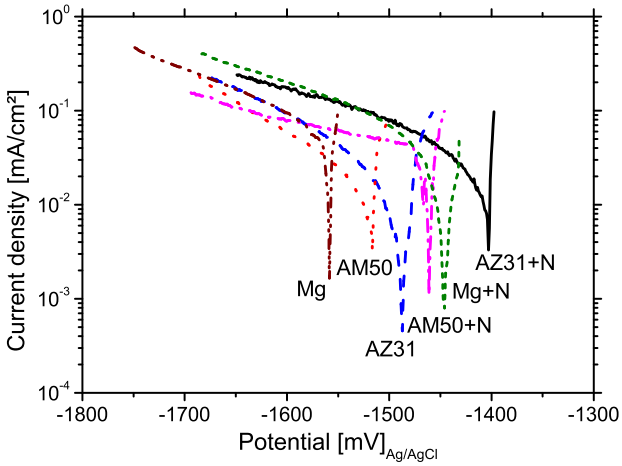

Figure 9: Potentiodynamic polarisation curves for the various untreated and implanted Mg alloys in 0.5% NaCl solution.

Unfortunately the results are not consistent with the findings of the EIS measurements. The typical Nyquist plots for each material/surface condition are displayed in Fig. 10 and the estimated charge transfer resistances are given in Tab. 2. Here improvements of the corrosion resistance are found for implanted CP-Mg but also for AM50. Both materials indicate a short term improvement of roughly one hour compared to the untreated alloy. It is obvious that the degradation starts more or less immediately after the exposure to the electrolyte. In contrast no improvement was noticed for the AZ31 alloy in the EIS measurements, which is consistent with the polarisation results of this alloy. Anyway after 4 hours the effects (regardless whether they were positive or negative) of the N implantation are more or less not visible anymore and implanted and as-received alloys have reached similar resistance values.

Due to the sensitivity of magnesium corrosion processes regarding impurities and surface properties the results have a rather large scatter in corrosion rates, thus it might be possible that the visible effects are still in the natural variation of the specimens. However there are a few points to mention keeping in mind that additional studies are required to confirm them:

1. Differences between polarisation and EIS measurements might be a result of the different times of measuring after immersion. For polarisation the measurement started 30 minutes after immersion and for EIS

Table 2: Change of charge transfer resistances (ctr) (Ωcm^2) as a function of immersion time in neutral 0.5% NaCl solution determined by EIS measurements.

time (h)/ctr (Ωcm^2)	CP-Mg	CP-Mg(N)	AZ31	AZ31(N)	AM50	AM50(N)
0	546	734	1183	722	1419	5918
1	297	252	1037	814	1512	2472
4	172	69	1026	934	1467	1494
10	105	45	1505	1100	1066	960
22	78	39	1063	964	581	733

more or less immediately or after 1 hour. The onset of degradation may vary from specimen to specimen and thus the results. Furthermore the cathodic charging during polarisation may have an additional effect.

2. There seems to be only a short term protection possible by N implantation
3. Regarding improvement of the corrosion resistance cast material (CP-Mg and AM50) appear to respond better on the N implantation compared to wrought material (AZ31). A possible explanation might be grain refinement of the coarse cast structure by the high energy ions. The wrought material has already a fine grain structure.
4. For the AM50 alloy, the improvement corrosion resistance might be also due to the formation of AlN (observed with XPS). This phenomenon does not occur strong for the AZ31 because of the lower aluminium content in this alloy.

3.4. Mechanical properties

The results of nano-indentation measurements are presented Fig. 11. Each material presents a hardness increase after nitrogen implantation, thanks to the formation of the Mg_3N_2 phase. The most significant relative increase was measured for the pure Mg: surface hardness rises from 0.8 to 3.2 GPa (+300% increase). For the aluminium containing alloys, a very high surface hardness was measured after nitrogen implantation: 4.2 GPa (AM50) and 5.4 GPa (AZ31). This high hardness is probably due to the formation of AlN.

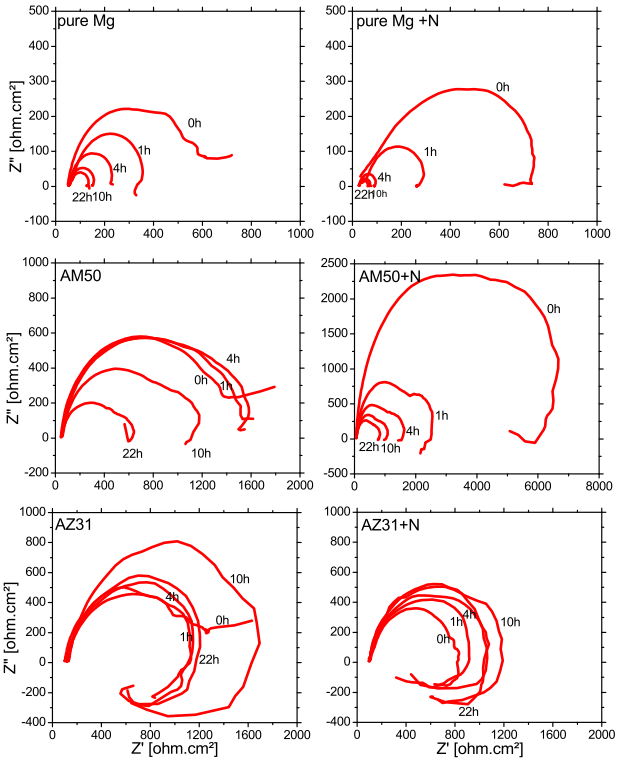

Figure 10: Time dependend development of the corrosion resistances (Nypuist plots) of the various untreated and implanted Mg alloys in 0.5% NaCl solution.

4. Conclusions

The experiments on nitriding magnesium and common Mg alloys by means of nitrogen ion implantation showed the successful formation of nanocrystalline Mg_3N_2 films to a thickness up to 600 nm. SIMS and XPS verifies the elemental distribution calculated by SRIM2008. Degradation of the nitride due to air humidity was avoided by means of a protective MgO passivation layer of about 150 nm thickness. The binding energy of N 1s atoms in Mg_3N_2 was measured to be 396.4 eV. In case of Mg 2p bonds the energy was determined at 50.3 eV. The aluminium containing alloys showed a better performance in corrosion and mechanical tests due to the formation of AlN.

In summary, the nitrogen ion implantation (Hardion$^+$) technology is a good tool to improve the mechanical surface properties of magnesium surfaces. In the case of corrosion protection some effects occur. The electrochemical potential was shifted for approx. 100 mV. For the aluminium containing alloys the corrosion properties have been improved for some hours, but altogether it is up to now not suitable for long tome corrosion protection. More implantation tests are needed to reach a long time corrosion protection.

References

[1] J. DeDamborenea, A. Conde, C. Palacio, R. Rodriguez, Modification of corrosion properties of titanium by N-implantation, Surface & Coatings Technology 91 (1997) 1–6.

[2] A. Jimenez Morales, J. C. Galvan, R. Rodriguez, J. J. De Damborenea, Electrochemical study of the corrosion behaviour of copper surfaces modified by nitrogen ion implantation, Journal of Applied Electrochemistry 27 (1997) 550–557.

[3] Y. Z. Liu, X. T. Zu, S. Zhu, L. M. Wang, Phase formation and corrosion behavior of nitrogen implanted Zr-Sn-Nb alloy in alkaline environment, Nuclear Instruments & Methods in Physics Research Section B-Beam Interactions with Materials and Atoms 246 (2006) 345–350.

[4] J. A. Garcia, A. Guette, A. Medrano, C. Labrugere, M. Rico, M. Lahaye, R. Sanchez, A. Martinez, R. J. Rodriguez, Nitrogen ion implantation on group IVb metals: chemical, mechanical and tribological study, Vacuum 64 (2002) 343–351.

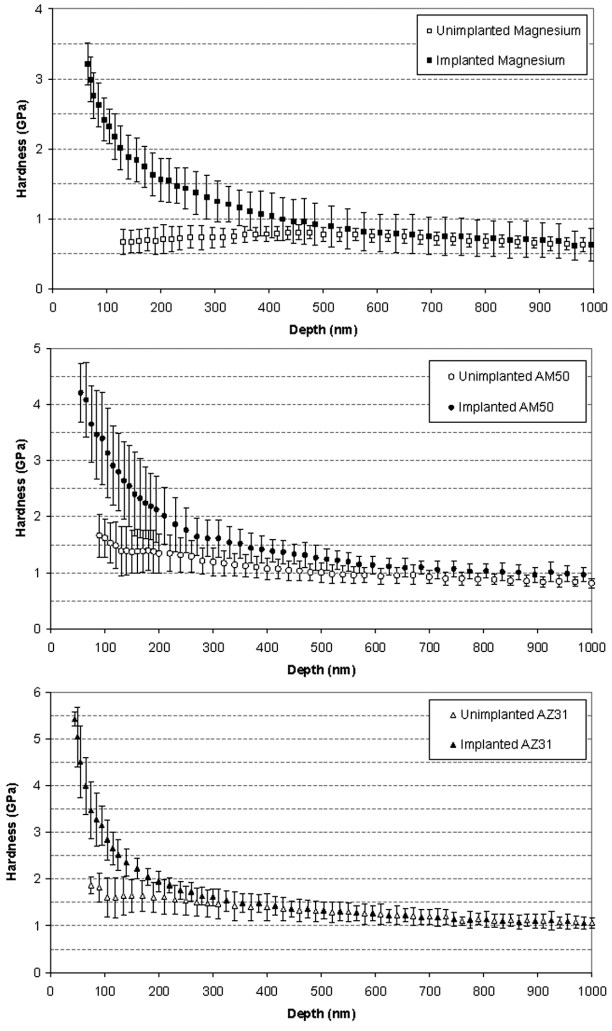

b

Figure 11: Hardness depth profiles measured by means of nanoindention technique applying Berkovich geometry.

[5] N. E. W. Hartley, Ion-Implantation and Surface Modification in Tribology, Wear 34 (1975) 427–438.

[6] E. Roman, J. L. Desegovia, R. Rodriguez, Mechanical-Properties of Steels Implanted with N2+, Vacuum 45 (1994) 1007–1008.

[7] R. J. Rodriguez, A. Sanz, A. Medrano, J. A. Garcia-Lorente, Tribological properties of ion implanted Aluminum alloys, Vacuum 52 (1999) 187–192.

[8] Y. Miyagawa, S. Nakao, M. Ikeyama, K. Saitoh, S. Miyagawa, Saturated thickness of nitride layers formed by high fluence nitrogen implantation into metals, Nuclear Instruments & Methods in Physics Research Section B-Beam Interactions with Materials and Atoms 127 (1997) 765–769.

[9] S. Ohira, M. Iwaki, Characterization of the Aluminum Surface-Layer Implanted with Nitrogen, Materials Science and Engineering 90 (1987) 143–148.

[10] P. Budzynski, P. Tarkowski, P. Penkala, Influence of nitrogen ion implantation on tribological properties of tool steel NC10, Vacuum 63 (2001) 731–736.

[11] D. M. Ruck, D. Boos, I. G. Brown, Improvement in Wear Characteristics of Steel Tools by Metal-Ion Implantation, Nuclear Instruments & Methods in Physics Research Section B-Beam Interactions with Materials and Atoms 80-1 (1993) 233–236.

[12] C. A. Straede, Application of ion implantation in tooling industry, Nuclear Instruments & Methods in Physics Research Section B-Beam Interactions with Materials and Atoms 113 (1996) 161–166.

[13] C. Blawert, N. Hort, K. U. Kainer, Automotive applications of magnesium and its alloys, Trans. Indian Inst. Met 57 (2004) 397–408.

[14] H. Dieringa, K. U. Kainer, Magnesium-der Zukunftswerkstoff fur die Automobilindustrie?, Materialwissenschaft und Werkstofftechnik 38 (2007) 91–96.

[15] B. L. Mordike, T. Ebert, Magnesium properties - applications - potential, Materials Science & Engineering A 302 (2001) 37–45.

[16] I. Nakatsugawa, R. Martin, E. Knystautas, Improving corrosion resistance of AZ91D magnesium alloy by nitrogen ion implantation, Corrosion 52 (1996) 921–926.

[17] G. Wu, K. Ding, X. Zeng, X. Wang, S. Yao, Improving corrosion resistance of titanium-coated magnesium alloy by modifying surface characteristics of magnesium alloy prior to titanium coating deposition, Scripta Materialia 61 (2009) 269–272.

[18] X. Tian, C. Wei, S. Yang, R. K. Fu, P. K. Chu, Corrosion resistance improvement of magnesium alloy using nitrogen plasma ion implantation, Surface and Coatings Technology 198 (2005) 454–458.

[19] J. Ziegler, J. Biersack, M. Ziegler, SRIM-2008 software package, 2008.

[20] X. Peng, D. Edwards, M. Barteau, Reactions of O2 and H2O with magnesium nitride films, Surface Science 195 (1988) 103–114.

[21] R. Dalmau, R. Collazo, S. Mita, Z. Sitar, X-Ray Photoelectron Spectroscopy Characterization of Aluminum Nitride Surface Oxides: Thermal and Hydrothermal Evolution, Journal of Electronic Materials 36 (2007) 414–419.

[22] G. Soto, J. A. Diaz, W. de la Cruz, A. Reyes, E. C. Samano, Amorphous magnesium nitride films produced by reactive pulsed laser deposition, Journal of Non-Crystalline Solids 342 (2004) 65–69.

[23] S. Ardizzone, C. Bianchi, M. Fadoni, B. Vercelli, Magnesium salts and oxide: an XPS overview, Applied Surface Science 119 (1997) 253–259.

[24] B. Timmermans, N. Vaeck, A. Hubin, F. Reniers, Chemical effects in Auger electron spectra of aluminium, Surf. Interface Anal. 34 (2002) 356–359.

[25] N. Fairley, Casaxps, version 2.3.15, Casa Software Ltd., Teighnmouth, Devon, UK (2008).

[26] B. Henke, E. Gullikson, J. Davis, X-ray interactions: photoabsorption, scattering, transmission, and reflection at E= 50-30,000 eV, Z= 1-92, Atomic data and nuclear data tables 54 (1993) 181–342.

[27] H. Klug, L. Alexander (Eds.), X-ray diffraction procedures: for polycrystalline and amorphous materials, WILEY, 1974.